Mechanism of Action of *N*-Acyl and *N*-Alkoxy Fosmidomycin Analogs: Mono- and Bisubstrate Inhibition of IspC from *Plasmodium falciparum*, a Causative Agent of Malaria

Misgina B. Girma, Haley S. Ball, Xu Wang, Robert C. Brothers, Emily R. Jackson, Marvin J. Meyers, Cynthia S. Dowd, and Robin D. Couch*
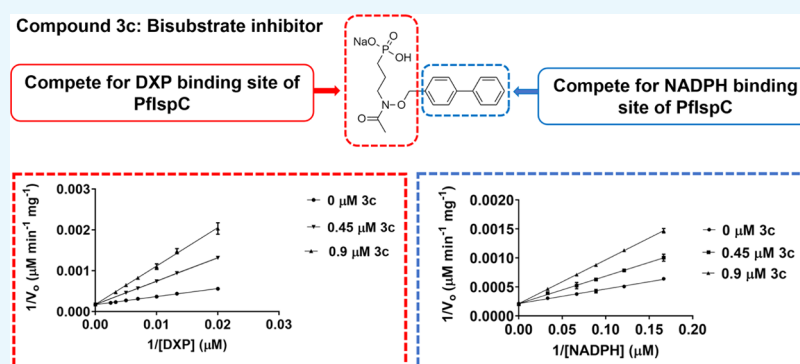
Cite This: *ACS Omega* 2021, 6, 27630−27639

Read Online

ACCESS | Metrics & More | Article Recommendations | Supporting Information

ABSTRACT: Malaria is a global health threat that requires immediate attention. Malaria is caused by the protozoan parasite *Plasmodium*, the most severe form of which is *Plasmodium falciparum*. The methylerythritol phosphate (MEP) pathway of isoprenoid biosynthesis is essential to the survival of many human pathogens, including *P. falciparum*, but is absent in humans, and thus shows promise as a new antimalarial drug target. The enzyme 1-deoxy-D-xylulose 5-phosphate reductoisomerase (IspC) catalyzes the first committed step in the MEP pathway. In addition to a divalent cation (Mg^{2+}), the enzyme requires the substrates 1-deoxy-D-xylulose 5-phosphate (DXP) and NADPH to catalyze its reaction. We designed *N*-alkoxy and *N*-acyl fosmidomycin analogs to inhibit the activity of *P. falciparum* IspC in a bisubstrate manner. Enzyme assays reveal that the *N*-alkoxy fosmidomycin analogs have a competitive mode of inhibition relative to both the DXP- and NADPH-binding sites, confirming a bisubstrate mode of inhibition. In contrast, the *N*-acyl fosmidomycin analogs demonstrate competitive inhibition with respect to DXP but uncompetitive inhibition with respect to NADPH, indicating monosubstrate inhibitory activity. Our results will have a positive impact on the discovery of novel antimalarial drugs.

INTRODUCTION

In 2017, an estimated 219 million cases of malaria occurred worldwide, with an estimated 435 000 malaria-associated deaths.[1] Of the various species of *Plasmodium* that cause malaria, *Plasmodium falciparum* is the most virulent.[2] This unicellular protozoan parasite is transmitted to humans via an infected mosquito, allowing the parasite to pass from the mosquito's saliva to the human bloodstream.[3] Once in the bloodstream, the parasites are carried to the liver, where they infect the liver cells. After multiplying in liver cells for 5−30 days, the parasite re-enters the bloodstream to continue its lifecycle.[4] Symptoms of malaria include fever, headache, and chills and if left untreated can result in death.[5] Currently, artemisinin-based combination therapies (ACTs) are first-line antimalarial treatments worldwide.[6] However, *P. falciparum* resistance to ACTs is spreading rapidly.[6] Therefore, there is an urgent need to develop new antibiotics to treat malaria.

The methylerythritol phosphate (MEP) pathway of isoprenoid biosynthesis has been identified as an important drug target, as it is essential for the survival of many human pathogens, including *P. falciparum*. Mammalian cells use a distinct isoprenoid pathway, known as the mevalonate (MVA) pathway, for the biosynthesis of isopentenyl pyrophosphate (IPP) and its isomer dimethylallyl pyrophosphate (DMAPP). IPP and DMAPP are building blocks of isoprenoids, molecules involved in several essential cellular functions.[7−9]
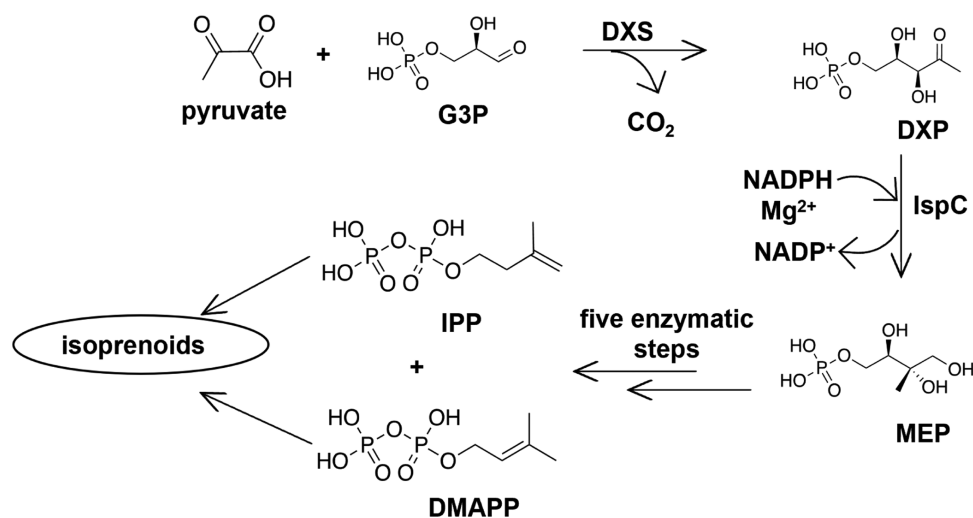
Figure 1. MEP pathway of isoprenoid biosynthesis. G3P: glyceraldehyde 3-phosphate; DXS: DXP synthase; IspC: 1-deoxy-D-xylulose 5-phosphate reductoisomerase; DXP: 1-deoxy-D-xylose 5-phosphate; MEP: 2-C-methyl-D-erythritol 4-phosphate; IPP: isopentenyl pyrophosphate; and DMAPP: dimethylallyl pyrophosphate.
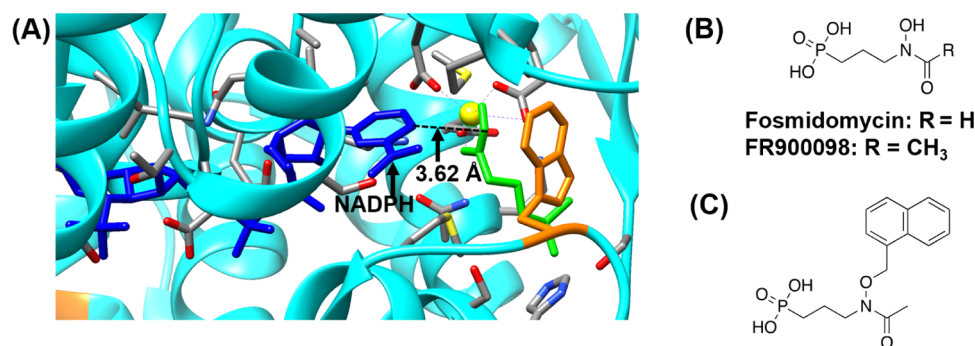

Figure 2. (A) Active site of *P. falciparum* IspC (PDB ID: 3AU9). NADPH is shown in blue, fosmidomycin in green, Mg^{2+} in yellow, and Trp296[15] in orange. FR900098 makes a bindentate interaction with Mg^{2+}. Amino acid labels are removed for clarity. The image was prepared using UCSF Chimera.[16] (B) Monosubstrate PfIspC inhibitors fosmidomycin and FR900098 (later labeled as **1a** and **2a** in Figure 3, respectively). (C) Previously reported bisubstrate inhibitor of IspC.[10] This *N*-alkoxy FR900098 analog is a more potent inhibitor of *Mycobacterium tuberculosis*, compared to the monosubstrate inhibitor FR900098.[10] Bisubstrate inhibitors are designed to bind to both the DXP site and the NADPH site.

The MEP pathway consists of seven enzymatically catalyzed steps (Figure 1) and is initiated by DXP synthase (DXS), catalyzing the formation of 1-deoxy-D-xylulose 5-phosphate (DXP) from pyruvate and glyceraldehyde 3-phosphate. 1-Deoxy-D-xylulose 5-phosphate reductoisomerase (IspC or DXR) is the second enzyme in the MEP pathway, catalyzing the first committed step of isoprenoid biosynthesis. Using NADPH and a divalent cation (Mg^{2+}), IspC converts DXP into 2-C-methylerythritol 4-phosphate (MEP). Sequentially, five additional enzymes convert MEP to the final MEP pathway products, IPP and DMAPP.[9,10]

In IspC, the NADPH-binding site is located adjacent to the DXP-binding site (Figure 2A). For the enzyme to carry out its activity, NADPH must bind first and induce a conformational change that facilitates the binding of DXP.[11] Fosmidomycin (FOS) and FR900098 (Figure 2B), natural products from *Streptomyces lavendulae* and *Streptomyces rubellomurinus*, respectively, are potent inhibitors of *P. falciparum* IspC (PfIspC) and effectively inhibit the growth of *P. falciparum*.[12] These inhibitors are competitive with respect to DXP (Figure 2A), targeting the DXP-binding site in IspC (i.e., they are monosubstrate inhibitors). Accordingly, FOS and FR900098 are uncompetitive inhibitors with respect to NADPH; NADPH

must bind to the NADPH site before FOS/FR900098 can bind to the DXP site.[10,13,14] Although FOS and FR900098 are potent inhibitors of PfIspC, they suffer from low bioavailability, short serum half-life, and malaria recrudescence.[10,12] Therefore, there is a need for novel analogs of FOS/FR900098 to overcome the shortcomings of these inhibitors.

We have reported previously the effectiveness of a bisubstrate inhibitor, designed to target the adjacent NADPH- and DXP-binding sites in IspC (Figure 2C).[10,13] The bisubstrate inhibitor demonstrated improved antibacterial activity relative to the monosubstrate inhibitors FOS/FR900098 (MIC = 25−200 μg/mL compared to MIC > 500 μg/mL, respectively).[10] Mechanistic investigations have revealed a "flip-and-lock" mechanism associated with the bisubstrate inhibitor, wherein inhibitor binding to the NADPH site causes a conformation change ("flip") in the active site of IspC, thereby forming the DXP site, which is then bound by the phosphonate side of the inhibitor ("lock").[10,11] Thus, a bisubstrate inhibitor is competitive with respect to both NADPH and DXP.[10]

The aim of the current study was to expand upon this initial work by rationally designing and synthesizing bisubstrate inhibitors of PfIspC. Two classes of inhibitors were prepared: *N*-acyl and *N*-alkoxy FOS analogs (Figure 3). Each class was

1a: R$_1$ = Na/H, R$_2$ = H
2a: R$_1$ = Na/H, R$_2$ = CH$_3$
3a: R$_1$ = Na/H, R$_2$ = n-butyl
4a: R$_1$ = Na/H, R$_2$ = CH$_2$(CH$_2$)$_2$Ph

1c: R$_1$= Na/H, R$_2$ = CH$_2$(4-iprPh)
2c: R$_1$= Na/H, R$_2$ = CH$_2$(1-naphthyl)
3c: R$_1$ = Na/H, R$_2$ = CH$_2$(4-biphenyl)

1b: R$_1$ = Na/H, R$_2$ = CH$_2$CH$_2$Ph
2b: R$_1$ = Na/H, R$_2$ = CH$_2$(CH$_2$)$_2$Ph

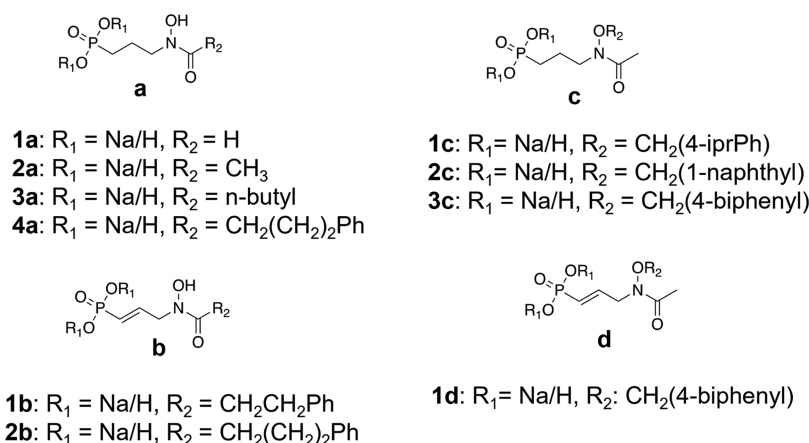**1d**: R$_1$= Na/H, R$_2$: CH$_2$(4-biphenyl)

Figure 3. *P. falciparum* IspC inhibitors: *N*-acyl (a, b) and *N*-alkoxy (c, d) fosmidomycin analogs. Natural products **1a** = fosmidomycin (FOS) and **2a** = FR900098. The *N*-acyl FOS analog **4a** is a saturated version of **2b**. Similarly, the *N*-alkoxy FOS analog **3c** is a saturated version of **1d**. All synthesized compounds were designed to act as bisubstrate inhibitors of IspC and tested as the monosodium salts.

Scheme 1. (a) Valeryl Chloride, TEA, and CH$_2$Cl$_2$; (b) 1 M BCl$_3$, CH$_2$Cl$_2$; and (c) TMSBr, *N*,*O*-Bis(trimethylsilyl)trifluoroacetamide, and CH$_2$Cl$_2$
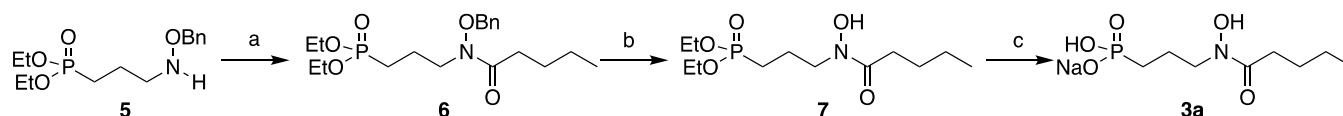
designed to act as a bisubstrate inhibitor, i.e., to be competitive with respect to both NADPH and DXP binding. As detailed herein, through the mechanism of inhibition assays, we ascertained that the *N*-alkoxy FOS analogs undergo a bisubstrate mode of inhibition. However, in contrast, the rationally designed *N*-acyl FOS analogs demonstrated a monosubstrate mode of inhibition, competitive with respect to DXP but uncompetitive with respect to NADPH. While the aromatic substituents of the *N*-acyl FOS analogs were expected to orient their *N*-acyl group toward the NADPH-binding site in IspC, our mechanism of inhibition data clearly indicates that the expected binding mode does not occur. Further, molecular modeling studies also support our findings, that the *N*-acyl FOS analogs preferentially position the *N*-acyl groups away from the NADPH site and thus are uncompetitive with respect to NADPH.

RESULTS AND DISCUSSION

Chemical Synthesis. The synthesis of compounds **4a**, **1c**, **2c**, **3c**, and **1d** was performed, as described previously.[12,13,17,18] The synthesis of compound **3a** is shown in Scheme 1. Briefly, acylation of compound **5**[10] was achieved using valeryl chloride and TEA to afford compound **6**. Debenzylation of **6** with boron trichloride gave hydroxyl amine **7**. Deprotection of phosphonate ester **7** using trimethylsilylbromide in the presence of BSTFA yielded desired target compound **3a**. Characterization of compounds **1b** and **2b** is given. The synthetic details will be reported elsewhere.

Mechanism of Inhibition of *N*-Alkoxy Fosmidomycin Analogs. To determine the mechanism of inhibition for these analogs, enzyme assays were performed using purified recombinant *P. falciparum* IspC and each inhibitor is listed in Figure 3. The results of the assays were plotted, as shown in Figure 4. As seen, the double reciprocal plots reveal that all of the *N*-alkoxy analogs (**1c**, **2c**, **3c**, and **1d**) behave as competitive inhibitors with respect to both DXP and NADPH, indicating that they function as bisubstrate inhibitors. Among these

analogs, the biphenyl compound (**3c**) is the most potent, with an inhibition constant (K_i) of 0.240 μM relative to DXP (Table 1). On the other hand, compound **1d**, the α,β-unsaturated version of compound **3c**, has a K_i value of 0.719 μM with respect to DXP (3-fold higher than that of **3c**). Similarly, saturated compound **1c** has a more potent K_i value (0.480 μM relative to DXP) than the structurally similar α,β-unsaturated compound, **1d** (0.719 μM). Therefore, it appears likely that the poorer K_i value of compound **1d** is, at least in part, due to the restriction imposed by the α,β-double bond, interfering with the binding of the phosphonate moiety of the inhibitor to the enzyme. Relative to NADPH, compound **3c** yields the lowest K_i value (K_i = 0.440 μM), while compound **1d** has the highest (K_i = 3.145 μM), again revealing the preference for the more flexible saturated backbone.

Mechanism of Inhibition of *N*-Acyl Fosmidomycin Analogs. The mechanism of inhibition experiments was carried out for the *N*-acyl fosmidomycin analogs in the same manner as for the *N*-alkoxys. As expected, all *N*-acyl fosmidomycin analogs (**FR900098**, **3a**, **4a**, **1b**, and **2b**) showed a competitive mode of inhibition relative to DXP (Figure 5). However, unlike the *N*-alkoxy analogs, all of the *N*-acyl analogs demonstrated an uncompetitive mode of inhibition relative to NADPH. Hence, NADPH binds to the enzyme before these inhibitors bind to the DXP site. While we hypothesized that the *N*-acyl moieties on compounds **3a**, **4a**, **1b**, and **2b** would extend into the NADPH site of *P. falciparum* IspC, it appears that they have adopted an alternative conformation (as discussed below).

FR900098 (**2a**) shows potent inhibition of IspC; the K_i value relative to the DXP site is 0.009 μM. Looking at the structure–activity relationships among the *N*-acyl analogs, substitution of the FR900098 methyl group with an n-butyl group (**3a**) significantly diminished the K_i relative to the DXP site (K_i = 0.009 μM for FR900098 vs K_i = 0.860 μM for **3a**). Interestingly, an even larger substituted group (**4a**) had less deleterious effect (K_i = 0.470 μM for **4a** vs 0.860 μM for **3a**). And, in contrast to
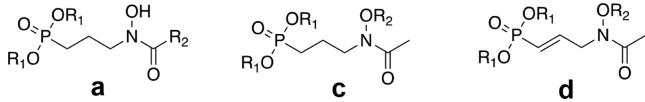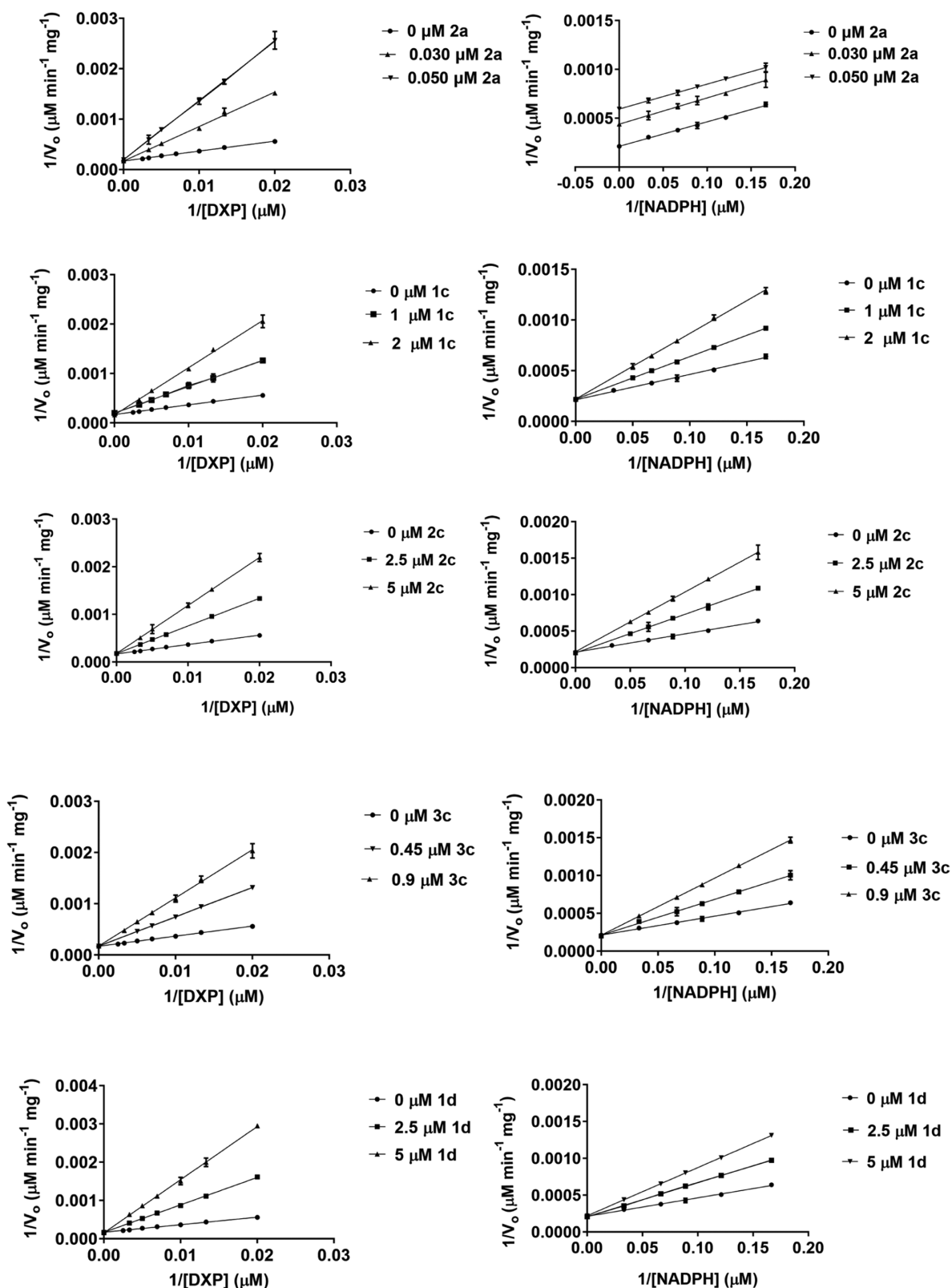
Figure 4. Lineweaver−Burk plots of the *N*-alkoxy fosmidomycin analogs. All four analogs (**1c**, **2c**, **3c**, and **1d**) demonstrate a competitive mode of inhibition with respect to both DXP and NADPH, indicating a bisubstrate mode of inhibition. FR900098 (**2a**), an *N*-acyl fosmidomycin analog, is presented for comparison; FR900098 is competitive with respect to DXP and uncompetitive with respect to NADPH. All assays were performed at least in triplicates with purified recombinant *P. falciparum* IspC.

the *N*-alkoxy analogs, which are less potent with *α,β*-unsaturation, the unsaturated *N*-acyl analogs performed better than their saturated counterparts (**1b** and **2b** vs **3a** and **4a**) (Table 2).

Table 1. Half-Maximal Inhibitory Concentration (IC_{50}) and Inhibition Constant (K_i) Values of N-Alkoxy Inhibitors Assayed Against *P. falciparum* IspC

compound	R_1	R_2	IC_{50} (μM)	$K_i{}^a$ (μM)	$K_i{}^b$ (μM)
1a = fosmidomycin	Na/H	H	0.034[12]	ND	NA
2a = FR900098	Na/H	CH$_3$	0.024[12]	0.009	NA
1c	Na/H	CH$_2$(4-iprPh)	1.411	0.480	1.217
2c	Na/H	CH$_2$(1-naphthyl)	3.361	1.166	2.195
3c	Na/H	CH$_2$(4-biphenyl)	0.804	0.240	0.440
1d	Na/H	CH$_2$(4-biphenyl)	5.670	0.719	3.145

^{a}Relative to DXP. ^{b}Relative to NADPH; ND: not determined; NA: not applicable. The inhibition constant (K_i) values are the results of the mechanism of inhibition (MoI) enzymatic assays performed at least in triplicate.

Docking Studies. Previously determined X-ray crystal structures of *P. falciparum* IspC have illustrated the structural flexibility of the active site loop in response to alternative binding modes of fosmidomycin analogs with bulky substituents.[19−21] In particular, positions of Trp296 and His293 change in response to binding analogs with bulky groups in the α- and β-positions (see Figure S6 and Table S1). Given this flexibility, we utilized four *P. falciparum* IspC crystal structures (PDB codes: 3AUA, 3WQR, 4Y67, and 4Y6R) with variable positioning of the loop and Trp296/His293 residues to conduct molecular docking studies to rationalize the difference in competitive vs uncompetitive binding with respect to NADPH for N-alkoxy and N-acyl inhibitors. The former two structures contain NADPH in the active site, while the latter two do not. Thus, docking models were created with and without NADPH for the former two structures giving six docking models.

To represent the N-alkoxy and N-acyl analogs, we selected compounds **3c** and **4a**, respectively, for docking. Briefly, the Glide docking routine in Schrodinger Maestro[22] was used to conduct flexible ligand docking in a rigid protein in an unbiased manner (i.e., no required contacts or binding with Mg^{2+} or other residues). Although docking of N-alkoxy **3c** produced reasonable poses in 5 of 6 docking models (Figure S7), it failed to produce any docked poses leading to bidentate binding of the inhibitor with Mg^{2+} except when docked in the 3AUA structure without the presence of NADPH (Figure 6). In this model, the N-alkoxy side chain binds in a mode that would be competitive with NADPH. Docking with unsaturated analog N-alkoxy **1d** produced virtually identical results and docked poses, as observed with **3c** (not shown). That supports the biochemical data showing **1d** binds in a mode competitive with NADPH. The α,β-unsaturated bond of **1d** located on the main chain of the inhibitor is one bond away from the phosphorus atom forming the phosphonate moiety, also located on the main chain of the inhibitor. However, this double bond is far from the N-alkoxy side chain (Figure 3). In addition, the N-alkoxy side chain of **1d** is not binding to the main chain of the inhibitor but to an oxygen atom with a single bond that allowed flexibility of the side chain. As a result, we anticipated that the α,β-unsaturated bond of **1d** would affect the binding of the phosphonate moiety of the inhibitor to the DXP-binding site but not significantly influence the orientiation of the N-alkoxy side chain relative to the NADPH-binding site. The K_i of **3c** and **1d** relative to the DXP are 0.240 and 0.719 μM, respectively. The observed difference in K_i relative to the DXP site between **3c**, the saturated N-alkoxy FOS analog, and **1d** is likely attributed to the presence of the

α,β-unsaturated bond of **1d**. In agreement with our anticipation, the biochemical assays and modeling studies revealed that both N-alkoxy compounds **3c** and **1d**, saturated and unsaturated, respectively, acted competitively with NADPH.

Docking of N-acyl **4a** produced satisfactory binding poses in all six docking models (Figure S8). Five of the docking models maintained the bidentate Mg^{2+} binding, including all four models where the NADPH site was unavailable for docking. Docking with the unsaturated analog N-acyl **2b** produced virtually identical results and docked poses, as observed with **4a** (example shown in Figure S9). This supports the biochemical data showing **4a** and **2b** to be uncompetitive with NADPH (i.e., they can bind by occupying the DXP site in the presence of NADPH (Figures 7 and S9)). The α,β-unsaturated bond of **2b** does not seem to affect the orientation of the N-acyl side chain relative to NADPH, since both the saturated **4a** and the unsaturated **2b** show uncompetitive mode relative to NADPH. It is likely that the orientation of the N-acyl side chains relative to the NADPH-binding site is mainly affected by the amide bond the side chains form.

It should be noted that we cannot make any definitive statements regarding precise positioning of N-alkoxy and N-acyl side chains other than to say it is likely that N-alkoxy compounds such as **3c** likely cannot form bidentate interaction with the Mg^{2+} except through displacement of NADPH (i.e., when the lipophilic group is buried deep in the binding site), while N-acyl compounds such as **4a** can adopt an alternative binding mode that may mimic other bulky substituents off the central propyl chain extending toward solvent.

CONCLUSIONS

Artemisinin-based combination therapies (ACTs) are already facing drug resistance by *P. falciparum*, therefore, there is an urgent need for novel antibiotics. Fosmidomycin is a potent inhibitor of *P. falciparum* IspC and *P. falciparum* growth, and clinical trials have shown that fosmidomycin is a remarkably safe drug in combination therapies. Nonetheless, fosmidomycin suffers from low bioavailability, short serum-life, and malaria recrudescence. We have designed, synthesized, and determined the mechanisms of inhibition of a series of N-acyl and N-alkoxy fosmidomycin analogs. We have shown that N-acyl fosmidomycin analogs do not inhibit *P. falciparum* IspC in a bisubstrate manner, possibly due to restrictions imposed by the amide bond. Molecular modeling revealed the N-acyl fosmidomycin analogs position their N-acyl groups away from the NADPH site and thus are uncompetitive relative to NADPH. We have shown that
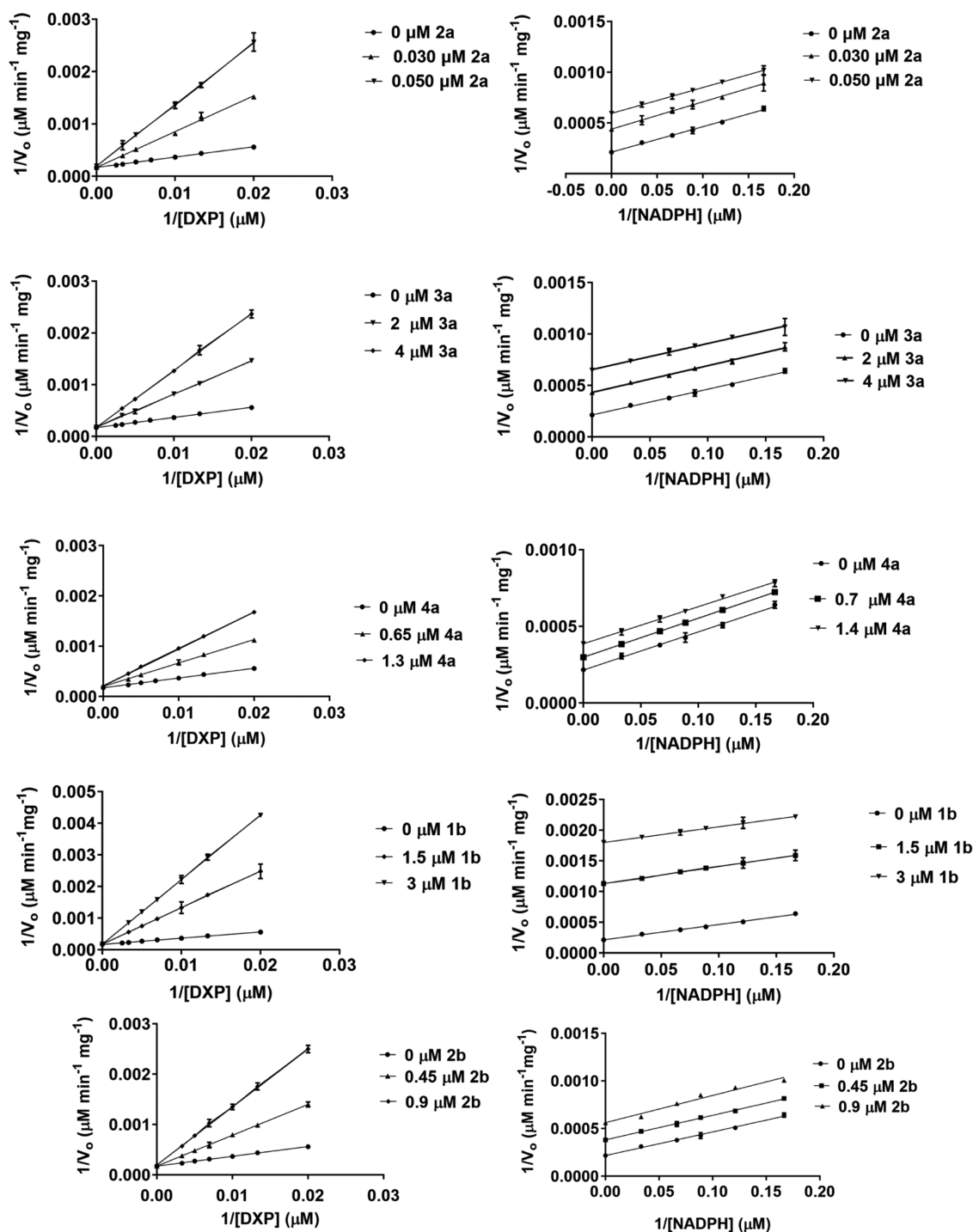
Figure 5. Lineweaver—Burk plots of the *N*-acyl fosmidomycin analogs. All five inhibitors (**2a** = FR900098, **3a**, **4a**, **1b**, and **2b**) show a competitive mode of inhibition against the DXP site of *P. falciparum* IspC but an uncompetitive mode of inhibition relative to the NADPH site. Bisubstrate inhibition was not observed for any of these *N*-acyl analogs. All assays were performed in at least in triplicate with purified recombinant *P. falciparum* IspC.

the *N*-alkoxy fosmidomycin analogs act in a bisubstrate mode of inhibition. Further study is warranted to develop additional compounds against *P. falciparum* IspC and to establish structure—activity relationships with various *N*-alkoxy and *N*-acyl moieties.

■ MATERIALS AND METHODS

Reagents and Chemical Synthesis. *General.* ^{1}H and ^{13}C NMR spectra were recorded in CDCl$_3$, CD$_3$OD, or D$_2$O on **an**

Agilent spectrometer at 400 and 100 MHz, respectively. ^{1}H and ^{13}C NMR spectra for one compound (**3a**) were recorded on an Agilent spectrometer at 200 and 50 MHz, respectively. TMS, H$_2$O, or solvent signal was used as internal standard. Chemical shifts are given in parts per million (ppm). Spin multiplicities are given with the following abbreviations: s (singulet), br s (broad singulet), d (doublet), dd (doublet of doublets), ddd (doublet of doublets of doublets), t (triplet), dt (doublet of triplets), ddt (doublet of doublet of triplets), q (quadruplet), qt (quintuplet),

Table 2. Half-Maximal Inhibitory Concentration (IC$_{50}$) and Inhibition Constant (K_i) Values of N-Acyl Inhibitors Assayed Against *P. falciparum* IspC

compound	R$_1$	R$_2$	IC$_{50}$ (μM)	K_i^a (μM)	K_i^b (μM)
1a = fosmidomycin	Na/H	H	0.034[12]	ND	NA
2a = FR900098	Na/H	CH$_3$	0.024[12]	0.009	NA
3a	Na/H	n-butyl	2.448	0.860	NA
4a	Na/H	CH$_2$(CH$_2$)$_2$Ph	1.344	0.470	NA
1b	Na/H	CH$_2$CH$_2$Ph	1.309	0.338	NA
2b	Na/H	CH$_2$(CH$_2$)$_2$Ph	0.900	0.162	NA

^{a}Relative to DXP. ^{b}Relative to NADPH; ND = not determined; NA = not applicable. The inhibition constant (K_i) values are the results of the mechanism of inhibition (MoI) enzymatic assays performed at least in triplicate.
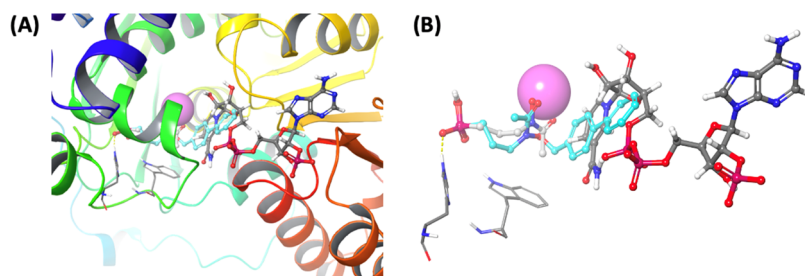

Figure 6. Docking model of N-alkoxy fosmidomycin analog **3c**. Analog **3c** was docked in *P. falciparum* IspC FR900098 structure 3AUA with NADPH pre-removed. FR900098, Trp296 and His293 are colored light gray. NADPH is colored dark gray. Mg^{2+} is colored magenta. Docked N-alkoxy analog **3c** is colored cyan. (A) Top scoring pose of **3c** overlaid on 3AUA structure. (B) Protein ribbons removed for clarity.
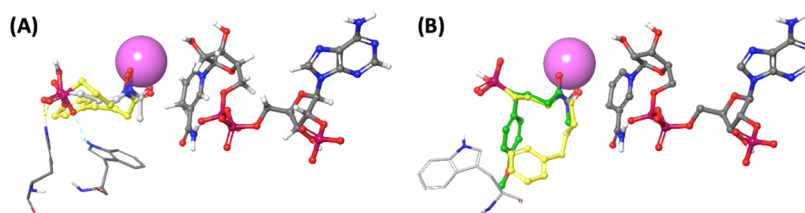

Figure 7. Docking models of N-acyl fosmidomycin analog **4a**. N-acyl analog **4a** was docked in *P. falciparum* IspC/FR900098 structure 3AUA with NADPH present (A) and 3WQR/α-Ph analog with NADPH present (B). FR900098, Trp296, and His293 are colored light gray. α-Ph analog from 3WQR is colored green. NADPH is colored dark gray. Mg^{2+} is colored magenta. Docked N-acyl analog **4a** is colored yellow.

and m (multiplet). Mass spectra were measured in the ESI mode on an HPLC-MS (Agilent 1100) or in the EI mode on a GC-MS (Shimadzu GC-MS-QP2010S). Thin-layer chromatography (TLC) was performed on Baker-flex Silica Gel IB2-F silica plates and flash column chromatography was carried out using SiliCycle SiliaFlash P60 silica gel (40−63 μm). All reagents were purchased from commercial suppliers and used without further purification. Anhydrous solvents were filtered by the MBRAUN MB-SPS solvent purification system before use. All air-sensitive reactions were carried out under a nitrogen atmosphere. The purity of synthesized compounds (>95%) was determined by ^{1}H/^{13}C NMR in combination with HPLC-MS (Agilent 1100). Column: Thermo Fisher Scientific Hypersil GOLD aQ C-18 3 μm particle (250 mm × 4.6 mm). Mobile phase (containing 0.1% formic acid as the additive): linear gradient of acetonitrile (50−100%) in water at a flow rate of 0.8 mL/min over 12.5 min, followed by 100% acetonitrile that was maintained for another 12.5 min. The UV detection wavelengths were 210 nm and 254 nm. High-resolution mass spectroscopy spectra (HRMS) were recorded in positive or negative ESI mode on a Waters Q-TOF Ultima mass spectrometer (UIUC Mass Spectrometry Labo-

ratory) or in positive FAB mode on a VG Analytical VG70SE magnetic sector mass spectrometer (JHU Mass Spectrometry Facility). Compound **5** was prepared, as previously described.[10]

1b: Sodium Hydrogen [(1E)-3-(N-hydroxy-3-phenylpropanamido)prop-1-en-1-yl]phosphonate. Light yellow solids (51 mg, 92%). ^{1}H NMR (400 MHz, D$_2$O) δ 7.26−7.09 (m, 5H), 6.29−6.13 (m, 1H), 5.77−5.59 (m, 1H), 4.22−4.11 (m, 2H), 2.85−2.66 (m, 4H). ^{13}C NMR (101 MHz, D$_2$O) δ 175.3, 140.7, 139.3 (d, J = 5.3 Hz), 128.7, 128.3, 126.4, 124.0 (d, J = 177.7 Hz), 50.8 (d, J = 23.6 Hz), 33.1, 30.2. LC-MS (ESI$^+$): 571.2 m/z [2M − 2Na + 3H]$^+$. HRMS (FAB$^+$) calculated for C$_{12}$H$_{15}$NNaO$_5$P, 307.0586; found, 308.0655 [M + H]$^+$.

2b: Sodium Hydrogen [(1E)-3-(N-hydroxy-4-phenylbutanamido)prop-1-en-1-yl]phosphonate. Light yellow solids (28 mg, 77%). ^{1}H NMR (400 MHz, CDCl$_3$) δ 7.12−7.25 (m, 5H), 6.30−6.41 (m, 1H), 5.75−5.85 (m, 1H), 4.22 (bs, 2H), 2.52−2.57 (m, 2H), 2.25 (t, J = 7.3 Hz, 2H), 1.76−1.83 (m, 2H). ^{13}C NMR (101 MHz, D$_2$O) δ 176.5, 142.1, 133.0 (d, J = 5.5 Hz), 130.4, 128.8, 126.3, 121.9 (d, J = 180.7 Hz), 50.9 (d, J = 23.5 Hz), 34.6, 31.2, 26.1. LC-MS (ESI$^+$): 300.0 m/z [M − Na

+ 2H]⁺, 599.2 m/z [2M − 2Na + 3H]⁺, 898.2 m/z [3M − 3Na + 4H]⁺. HRMS (FAB⁺) calculated for $C_{13}H_{17}NNaO_5P$, 321.0742; found, 322.0862 [M + H]⁺.

3a: *Sodium Hydrogen-3-(N-hydroxypentanamido)-propylphosphonate.* N,O-Bis(trimethylsilyl)-trifluoroacetamide (0.15 mL, 0.145 g, 0.56 mmol) was added under a nitrogen atmosphere to diethyl 3-(N-hydroxypentanamido)propylphosphonate (**7**) (0.050 g, 0.17 mmol) in CH_2Cl_2 (0.75 mL) and stirred at room temperature for 20 min. The reaction mixture was cooled to 0°C and bromotrimethylsilane (0.22 mL, 0.255 g, 1.67 mmol) was added dropwise to the reaction. The reaction was warmed to room temperature and stirred overnight under a nitrogen atmosphere. Ethyl bromide and excess silylating agent were removed under reduced pressure and the residue was dissolved in aqueous NaOH (0.86 mL, 7.8 mg/mL) and stirred for a 2nd night. The reaction mixture was partitioned between H_2O and CH_2Cl_2 to remove any residual impurities/organics. The aqueous fractions were combined, and the solvent was removed by lyophilization to give **3a** (0.049 g, 0.18 mmol, Quantitative) as a pale-yellow solid. ¹H NMR (200 MHz, acetone-d_6/D_2O) δ (ppm): 3.72−3.62 (m, 2H), 2.55 (t, J = 7.7 Hz, 2H),2.07−1.77 (m, 2H), 1.61 (p, J = 8.3, 7.8 Hz, 4H), 1.39 (h, J = 13.8, 7.1 Hz, 2H), 0.95 (t, J = 7.4 Hz, 3H). ¹³C NMR (50 MHz, acetone-d_6/D_2O) δ (ppm): 176.33, 49.00 (d, J = 18.8 Hz), 32.01, 27.02, 24.11, 22.30, 21.09, 13.52. LC-MS (ESI) m/z 240.1 (M + H). HRMS (ESI) m/z calcd for $C_8H_{17}NO_5P$ (M − Na): 238.0838, found: 238.0833.

7: *Diethyl 3-(N-hydroxypentanamido)-propylphosphonate.* A solution of **6** (0.208 g, 0.54 mmol) in dry CH_2Cl_2 (10.0 mL) was cooled to −50 °C and a 1 M solution of BCl_3 in CH_2Cl_2 (3.5 mL, 3.5 mmol) was added dropwise. After stirring for 4 h at −50 °C, the reaction was quenched with saturated $NaHCO_3$ (aq, 16 mL) and warmed to room temperature. The aqueous reaction mixture was extracted with CH_2Cl_2 (×3). The organic fractions were combined, dried over $MgSO_4$, and filtered and the solvent was removed under reduced pressure. The resulting crude mixture was purified using an Isolera Flash Chromatography System (EtOAc/MeOH; 5−10% MeOH) to yield **7** (0.125 g, 0.42 mmol, 78.5%) as a yellow oil. ¹H NMR (200 MHz, $CDCl_3$) δ (ppm): 9.53 (s, ¹H), 4.06 (p, J = 6.9 Hz, 4H), 3.74 (t, J = 5.6 Hz, 2H), 2.51 (t, J = 7.7 Hz, 2H), 2.10−1.90 (m, 2H), 1.88−1.71 (m, 2H), 1.61 (p, J = 7.4 Hz, 2H), 1.47−1.36 (m, 2H), 1.32 (t, J = 7.1 Hz, 7H), 0.91 (t, J = 7.3 Hz, 3H). ¹³C NMR (50 MHz, $CDCl_3$) δ (ppm): 175.31, 62.16 (d, J = 7.2 Hz), 47.81, 32.30, 26.89, 23.72, 22.66, 19.34, 16.42 (dd, J = 3.2 Hz), 13.92. LC-MS (ESI) m/z 296.2 (M + H).

6: *Diethyl 3-[N-(benzyloxy)pentanamido]-propylphosphonate.* To a stirred solution of **5** (0.203 g, 0.66 mmol) and triethylamine (0.2 mL, 0.14 g, 1.3 mmol) in CH_2Cl_2 (3 mL) at room temperature and under an argon atmosphere was added valeryl chloride (0.1 mL, 0.097 g, 0.8 mmol) dropwise. The reaction mixture was stirred at room temperature overnight. The reaction mixture was extracted with water and brine. The aqueous layer was back-extracted with CH_2Cl_2 (×3) and dried over anhydrous magnesium sulfate. The magnesium sulfate was filtered from the organic layer and the solvent was removed under reduced pressure. The crude residue was purified using an Isolera Flash Chromatography (100% EtOAc) to give **6** (0.207 g, 0.54 mmol, 81.4%) as a yellow oil. ¹H NMR ($CDCl_3$, 200 MHz), δ (ppm): 7.38 (s, 5Harom), 4.81 (s, 2H), 4.08 (p, J = 7.3 Hz, 4H), 3.71 (t, J = 6.8 Hz, 2H), 2.39 (t, J = 7.6 Hz, 2H), 2.03−1.48 (m, 6H), 1.75−1.60 (m, 2H), 1.30 (t, J =

6.2 Hz, 6H), 1.37−1.24 (m, 2H). LC-MS (ESI) m/z 486.2 (M + H).

Expression and Purification of *P. falciparum* IspC. The cloning, expression, and purification of *P. falciparum* IspC were performed, as described previously.[10,12,17] Briefly, the *P. falciparum* IspC gene was cloned into a pET100/D-TOPO vector to facilitate the expression of an N-terminal His₆-tagged protein. The recombinant protein was expressed in *Escherichia coli* Rosetta2(DE3) cells obtained from Novagen (San Diego, CA). *E. coli* was cultured at 37 °C in Luria-Bertani media supplemented with 100 µg/mL ampicillin and 34 µg/mL chloramphenicol with constant shaking at 250 rpm. Agar (1.5% w/v) was added to prepare solid media. Protein was isolated and purified from the cells via chemical lysis and TALON affinity chromatography (Clontech Laboratories, Mountain View, CA).

P. falciparum IspC Inhibition Assays. The IspC activity was assayed at 37 °C by spectrophotometrically monitoring the enzyme-catalyzed oxidation of NADPH, as described previously.[12,13,17] Briefly, the assay mixture contained 100 mM Tris pH 7.8, 25 mM $MgCl_2$, and 0.86 µM *P. falciparum* IspC. To determine the half-maximal inhibition (IC_{50}) concentrations, the enzyme was preincubated with the inhibitor for 10 min at 37 °C prior to the addition of 150 µM NADPH. The reaction mixture was further incubated for 5 min at 37 °C. The reaction was initiated with the addition of 144 µM DXP (Echelon Biosciences, Salt Lake City, UT) to the assay mixture. The oxidation of NADPH was monitored at 340 nm using an Agilent 8453 UV−visible spectrophotometer equipped with a temperature-regulated cuvette holder. One unit of *P. falciparum* IspC activity is defined as the amount of enzyme that catalyzes the oxidation of 1 µM NADPH per min per mg of the enzyme. Half-maximal inhibition (IC_{50}) of enzyme activity was determined using a plot of fractional enzyme activity as a function of inhibitor concentration. Nonlinear regression of the sigmoidal dose−response curve was generated using GraphPad Prism version 7.00 for Windows (GraphPad Software Inc., San Diego, CA). All enzymatic assays performed to determine half-maximal inhibition concentration (IC_{50}) of an inhibitor were performed in duplicate. All IC_{50} values were validated by a second enzymologist performing an inhibition assay (data not shown) with the inhibitor at the IC_{50} concentration, confirming 50% residual enzyme activity (±5%).

To determine the mechanism of inhibition (MoI), the enzyme assay was performed as described above with varying concentrations of DXP and NADPH. To determine the MoI with respect to the DXP-binding site, the DXP concentration was varied between 50 and 400 µM, while the NADPH concentration was kept constant at 150 µM. To determine the MoI with respect to the NADPH-binding site, the NADPH concentration was varied between 6 and 30 µM, while the DXP concentration was kept constant at 144 µM. The MoI was determined using Lineweaver−Burk plots; linear regression of the data was generated using GraphPad Prism. The inhibitor constants (K_i values) were determined by generating secondary plots from the Lineweaver−Burk plots; linear regression of the data was generated using GraphPad Prism. All of the MoI assays were performed at least in triplicate.

Molecular Modeling Studies. Modeling studies were conducted with Schrodinger Maestro Release 2019-4.[22] Crystal structures 3AUA, 3WQR, 4Y6R, and 4Y67 were imported from the Protein Data Bank (PDB)[23] and prepared using Protein Preparation Wizard. Glide docking grids were generated from these structures removing the bound ligand while placing no

restrictions or constraints on the ligand binding protocol. For structures 3AUA and 3WQR, a second Glide docking grid was generated wherein the NAPDH and associated water molecules were removed before grid generation. Glide docking was performed using these six docking grids under the XP precision mode and all other defaults with the exception of increasing the number of output structures to three per docked compound.

■ ASSOCIATED CONTENT

Ⓢ Supporting Information

The Supporting Information is available free of charge at https://pubs.acs.org/doi/10.1021/acsomega.1c01711.

Inhibition constant (K_i) values and half-maximal inhibitory concentration (IC_{50}) plots molecular modeling studies (PDF)

Molecular formula strings (XLSX)

■ AUTHOR INFORMATION

Corresponding Author

Robin D. Couch − Department of Chemistry and Biochemistry, George Mason University, Manassas, Virginia 20110, United States; Email: rcouch@gmu.edu

Authors

Misgina B. Girma − Department of Chemistry and Biochemistry, George Mason University, Manassas, Virginia 20110, United States; ● orcid.org/0000-0002-5510-0514

Haley S. Ball − Department of Chemistry and Biochemistry, George Mason University, Manassas, Virginia 20110, United States

Xu Wang − Progenra Inc., Malvern, Pennsylvania 19355, United States; ● orcid.org/0000-0001-7379-5789

Robert C. Brothers − Department of Chemistry, The George Washington University, Washington, District of Columbia 20052, United States

Emily R. Jackson − Department of Chemistry, The George Washington University, Washington, District of Columbia 20052, United States

Marvin J. Meyers − Department of Chemistry, Saint Louis University, Saint Louis, Missouri 63103, United States

Cynthia S. Dowd − Department of Chemistry, The George Washington University, Washington, District of Columbia 20052, United States

Complete contact information is available at:
https://pubs.acs.org/10.1021/acsomega.1c01711

Notes

The authors declare no competing financial interest.

■ ACKNOWLEDGMENTS

■ REFERENCES

(1) WHO. World Malaria Report 2018. http://www.who.int/malaria/publications/world-malaria-report-2018/report/en/ (accessed October 31, 2019).

(2) Hayward, R. E.; Tiwari, B.; Piper, K. P.; Baruch, D. I.; Day, K. P. Virulence and Transmission Success of the Malarial Parasite *Plasmodium falciparum*. *Proc. Natl. Acad. Sci. U.S.A.* **1999**, *96*, 4563−4568.

(3) CDC. About Malaria − Biology. https://www.cdc.gov/malaria/about/biology/index.html (accessed November 2, 2019).

(4) Soulard, V.; Bosson-Vanga, H.; Lorthiois, A.; Roucher, C.; Franetich, J.-F.; Zanghi, G.; Bordessoulles, M.; Tefit, M.; Thellier, M.; Morosan, S.; Le Naour, G.; Capron, F.; Suemizu, H.; Snounou, G.; Moreno-Sabater, A.; Mazier, D. *Plasmodium falciparum* Full Life Cycle and *Plasmodium ovale* Liver Stages in Humanized Mice. *Nat. Commun.* **2015**, *6*, No. 7690.

(5) World Malaria Report 2019. https://www.who.int/publications-detail-redirect/world-malaria-report-2019 (accessed June 30, 2020).

(6) Ouji, M.; Augereau, J.-M.; Paloque, L.; Benoit-Vical, F. *Plasmodium falciparum* Resistance to Artemisinin-Based Combination Therapies: A Sword of Damocles in the Path toward Malaria Elimination. *Parasite* **2018**, *25*, No. 24.

(7) Heuston, S.; Begley, M.; Gahan, C. G. M.; Hill, C. Isoprenoid Biosynthesis in Bacterial Pathogens. *Microbiology* **2012**, *158*, 1389−1401.

(8) Holstein, S. A.; Hohl, R. J. Isoprenoids: Remarkable Diversity of Form and Function. *Lipids* **2004**, *39*, 293−309.

(9) Hoshino, Y.; Gaucher, E. A. On the Origin of Isoprenoid Biosynthesis. *Mol. Biol. Evol.* **2018**, *35*, 2185−2197.

(10) San Jose, G.; Jackson, E. R.; Haymond, A.; Johny, C.; Edwards, R. L.; Wang, X.; Brothers, R. C.; Edelstein, E. K.; Odom, A. R.; Boshoff, H. I.; Couch, R. D.; Dowd, C. S. Structure−Activity Relationships of the MEPicides: N-Acyl and O-Linked Analogs of FR900098 as Inhibitors of Dxr from *Mycobacterium tuberculosis* and *Yersinia pestis*. *ACS Infect. Dis.* **2016**, *2*, 923−935.

(11) Koppisch, A. T.; Fox, D. T.; Blagg, B. S. J.; Poulter, C. D. *E. coli* MEP Synthase: Steady-State Kinetic Analysis and Substrate Binding. *Biochemistry* **2002**, *41*, 236−243.

(12) Wang, X.; Edwards, R. L.; Ball, H.; Johnson, C.; Haymond, A.; Girma, M.; Manikkam, M.; Brothers, R. C.; McKay, K. T.; Arnett, S. D.; Osbourn, D. M.; Alvarez, S.; Boshoff, H. I.; Meyers, M. J.; Couch, R. D.; Odom John, A. R.; Dowd, C. S. MEPicides: α,β-Unsaturated Fosmidomycin Analogues as DXR Inhibitors against Malaria. *J. Med. Chem.* **2018**, *61*, 8847−8858.

(13) San Jose, G.; Jackson, E. R.; Uh, E.; Johny, C.; Haymond, A.; Lundberg, L.; Pinkham, C.; Kehn-Hall, K.; Boshoff, H. I.; Couch, R. D.; Dowd, C. S. Design of Potential Bisubstrate Inhibitors against *Mycobacterium tuberculosis* (Mtb) 1-Deoxy-D-Xylulose 5-Phosphate Reductoisomerase (Dxr)-Evidence of a Novel Binding Mode. *MedChemComm* **2013**, *4*, 1099−1104.

(14) Jackson, E. R.; Dowd, C. S. Inhibition of 1-Deoxy-D-Xylulose-5-Phosphate Reductoisomerase (Dxr): A Review of the Synthesis and Biological Evaluation of Recent Inhibitors. *Curr. Top. Med. Chem.* **2012**, *12*, 706−728.

(15) RCSB PDB 3AU9: Crystal Structure of the Quaternary Complex-1 of an Isomerase. https://www.rcsb.org/structure/3AU9 (accessed August 11, 2020).

(16) UCSF Chimera Home Page. https://www.cgl.ucsf.edu/chimera/ (accessed July 10, 2020).

(17) Haymond, A.; Johny, C.; Dowdy, T.; Schweibenz, B.; Villarroel, K.; Young, R.; Mantooth, C. J.; Patel, T.; Bases, J.; Jose, G. S.; Jackson, E. R.; Dowd, C. S.; Couch, R. D. Kinetic Characterization and Allosteric Inhibition of the Yersinia Pestis 1-Deoxy-D-Xylulose 5-Phosphate Reductoisomerase (MEP Synthase). *PLoS One* **2014**, *9*, No. e106243.

(18) Wang, X.; Dowd, C. S. The Methylerythritol Phosphate Pathway: Promising Drug Targets in the Fight against Tuberculosis. *ACS Infect. Dis.* **2018**, *4*, 278−290.

(19) Chofor, R.; Sooriyaarachchi, S.; Risseeuw, M. D. P.; Bergfors, T.; Pouyez, J.; Johny, C.; Haymond, A.; Everaert, A.; Dowd, C. S.; Maes, L.;

Coenye, T.; Alex, A.; Couch, R. D.; Jones, T. A.; Wouters, J.; Mowbray, S. L.; Van Calenbergh, S. Synthesis and Bioactivity of β-Substituted Fosmidomycin Analogues Targeting 1-Deoxy-d-Xylulose-5-Phosphate Reductoisomerase. *J. Med. Chem.* **2015**, *58*, 2988−3001.

(20) Umeda, T.; Tanaka, N.; Kusakabe, Y.; Nakanishi, M.; Kitade, Y.; Nakamura, K. T. Molecular Basis of Fosmidomycin's Action on the Human Malaria Parasite *Plasmodium falciparum. Sci. Rep.* **2011**, *1*, No. 9.

(21) Konzuch, S.; Umeda, T.; Held, J.; Hähn, S.; Brücher, K.; Lienau, C.; Behrendt, C. T.; Gräwert, T.; Bacher, A.; Illarionov, B.; Fischer, M.; Mordmüller, B.; Tanaka, N.; Kurz, T. Binding Modes of Reverse Fosmidomycin Analogs toward the Antimalarial Target IspC. *J. Med. Chem.* **2014**, *57*, 8827−8838.

(22) Schrödinger. Announcing Schrödinger Software Release 2019-4. https://www.schrodinger.com/user-announcement/announcing-schrodinger-software-release-2019-4 (accessed June 1, 2020).

(23) RCSB PDB: Homepage. https://www.rcsb.org/ (accessed November 29, 2019).